JMEPEG (2023) 32:7004–7015
https://doi.org/10.1007/s11665-022-07598-3

©The Author(s)
1059-9495/$19.00

TECHNICAL ARTICLE

Non-destructive Evaluation of Workpiece Properties along the Hybrid Bearing Bushing Process Chain

Lara Vivian Fricke, Susanne Elisabeth Thürer, Christoph Kahra, Susanne Bährisch, Sebastian Herbst, Florian Nürnberger, Bernd-Arno Behrens, Hans Jürgen Maier, Christian Klose, and Sebastian Barton

Submitted: 23 June 2022 / Revised: 27 September 2022 / Accepted: 17 October 2022 / Published online: 9 November 2022

To combine the advantages of two materials, hybrid bulk metal workpieces are attractive for subsequent processes such as metal forming. However, hybrid materials rely on the initial bond strength for the effective transfer of applied loads. Thus, a non-destructive evaluation of the bonding along the production process chain is of high interest. To evaluate to what extent non-destructive testing can be employed to monitor the bonding quality between the joining partners steel and aluminum and to characterize the age hardening condition of the aluminum component, ultrasonic testing and electrical conductivity measurements were applied. It was found that a lateral angular co-extrusion process can create homogeneous bonding although the electrical conductivity of the aluminum is altered during processing. A previous bonding before the subsequent die forging process leads to a sufficient bonding in areas with little deformation and is therefore, advantageous compared to unjoined semi-finished products, which do not form a bonding if the deformation ratio is too small. An influence of the subsequent heat treatment on the bonding is not visible in the ultrasonic testing signals though a homogenized electrical conductivity can be detected, which indicates uniform artificial aging conditions of the aluminum alloy

Keywords aluminum, bond evaluation, hybrid bulk metal component, non-destructive testing, process chain monitoring, steel, tailored forming

1. Introduction

Non-destructive testing (NDT) is an important tool in Industry 4.0 to enhance the sustainability, safety and product quality of production processes (Ref 1). Following that, well-established NDT techniques could also be used lead to an improvement of new production processes. Newly developed components must have properties such as a compact design, low weight and enhanced functionality with respect to lifetime. To meet these challenges and to reduce weight to save energy and CO_2 emissions, hybrid bulk material components are promising (Ref 2). Currently, a number of different production processes are applied to produce hybrid components like metal arc joining (Ref 3), vacuum rolling (Ref 4), laser welding (Ref 5) or friction welding (Ref 6-8). Typically, the different materials are joined at the end of the manufacturing process. There are also processes such as tailored blanks where the joining of two materials takes place before the forming process. A tailored blank is a sheet metal blank that is typically composed of different material grades and sheet thicknesses. This prefabricated semi-finished product is then formed into the desired component by deep drawing. By contrast, within the Collaborative Research Centre (CRC) 1153, aluminum and steel are combined in the first production step to produce load-adjusted hybrid solid components with wear-resistant functional surfaces (Ref 9, 10). This new approach allows for a greater degree of control over the evolution of the interfacing microstructure along the whole process chain. These process chains, where the materials are joined in the first production process, are challenging due to the different material properties. Often, at least one material must be manufactured close to its processing limits. To enhance the production of hybrid bulk materials knowledge of the current material and joining status in each process step is crucial to be able to adapt each process step to tailor the desired components properties. Non-destructive testing methods are suitable to characterize microstructures and bonding states. Generally, non-destructive testing methods are increasingly used to monitor industrial processes due to the increasing need in establishing the integrity and reliability of engineering materials and parts (Ref 11).

Regarding the process design, numerical simulations can be instrumental in identifying suited process parameters and to predict the resulting interface and microstructure (Ref 9). However, to improve the existing numerical models regarding the influencing parameters and to enhance the process understanding, it is important to increase the quality of the input data. In this context, non-destructive testing performed after individual process steps can provide important information regard-

Lara Vivian Fricke, Susanne Elisabeth Thürer, Christoph Kahra, Sebastian Herbst, Florian Nürnberger, Hans Jürgen Maier, Christian Klose, and **Sebastian Barton**, Institut für Werkstoffkunde (Institute for Materials Science), Leibniz Universität Hannover, 30823 Garbsen, Germany; **Susanne Bährisch** and **Bernd-Arno Behrens**, Institut für Umformtechnik und Umformmaschinen (Institute of Forming Technology and Machines), Leibniz Universität Hannover, 30823 Garbsen, Germany. Contact e-mails: fricke@iw.uni-hannover.de, thuerer@iw.uni-hannover.de, kahra@iw.uni-hannover.de, baehrisch@ifum.uni-hannover.de, herbst@iw.uni-hannover.de, nuernberger@iw.uni-hannover.de, behrens@ifum.uni-hannover.de, maier@iw.uni-hannover.de, klose@iw.uni-hannover.de, and barton@iw.uni-hannover.de.

ing material bonding and microstructure evolution toward manufacturing defect-free hybrid components. The non-destructively gathered data allow conclusions to be drawn about the component conditions and also permits targeted adjustment of individual process steps.

Hybrid products manufactured by Tailored Forming are required to have a firm bond between the joining partners to withstand the loads occurring during their life cycle. Since debonding between dissimilar materials is one of the most critical failure modes, it is important to understand the mechanisms for forming a material bond to ensure the safe and reliable use of such hybrid structures in a variety of applications. One approach to characterize the bonding properties and identify the influence of the processing parameters on the properties of hybrid bulk metal components is to analyze the bonding properties after each production step by destructive testing methods like metallographic examinations and tensile tests (Ref 12). Though this can be very useful, it is time-consuming, and thus usually only a few number of samples can be analyzed. In contrast, non-destructive testing methods can be applied instead to monitor the workpiece property evolution along the process chain or during its life cycle (Ref 13-16). With such an approach, process knowledge regarding the influencing parameters will be gained and a step-to-step optimization is achievable.

To evaluate the suitability of a non-destructive monitoring in a process chain, hybrid bearing bushings were produced by Tailored Forming according to Thürer et al. (Ref 17). The bonding between aluminum and steel was characterized by ultrasonic testing along the process chain so that the influence of each production step on the bonding gets obvious and not only the bonding condition at the end of the process chain. Additionally, the electrical conductivity was measured to determine microstructural changes from process step to process step. In previous investigations, Thürer et al. (Ref 17) observed that segments of the bearing bushings did not always form a continuous joining zone. Additionally, longitudinal weld seams (LWS) were observed after the LACE process. LWS are the joints that are created by re-welding the aluminum streams divided in the die. The formation of LWS is a solid-state bonding process for all profiles produced with chamber tools and porthole dies. The quality of the LWS can be attributed to the thermomechanical conditions (*e.g.*, temperature, pressure) inside the tool (Ref 18). Furthermore, the quality of the two surfaces of the metal streams is decisive for the resulting properties of the LWS. Due to the LWS, different microstructures and locally varying mechanical properties can be present in the profile. Thus, it is useful to detect and located the LWS for the following process steps by non-destructive testing since cracks are likely to occur at the LWS within the die forging process. Knowing the position of the LWS, an adaption of the process parameters of the following process steps might be possible to avoid cracking.

For the given task, the joining zone was non-destructively monitored by ultrasonic testing along the process chain. Ultrasonic testing is commonly used to analyze thin coatings on metals regarding their characteristics and possible cracks or debonded areas (Ref 19, 20). This technology is a suitable and well-known method to characterize joints for various materials (Ref 21-24). In addition, the microstructure evolution (*i.e.*, the artificial aging) of aluminum alloys can be monitored by measurements of the electrical conductivity by eddy current testing (Ref 25-28). Thus, both these two methods were applied to foster the process knowledge by analyzing the bonding between steel and aluminum alloy and characterizing the electric conductivity related to the precipitation hardening in the aluminum alloy for three different process steps within the Tailored Forming process chain. The aim is to ensure a high workpiece quality excluding any debonding at an early stage of the process chain of the production.

2. Materials and Methods

2.1 Process Chain

The process chain for manufacturing hybrid solid components using Tailored Forming is divided into the following steps. LACE was used as the first step to produce hybrid semi-finished workpieces in the form of steel-aluminum profiles, which were then segmented for the following die forging process. Subsequently to the die forging which forms the bushings, a heat treatment was carried out and the bushings were machined into their final shape. The whole process chain is displayed in Fig. 1. Non-destructive testing methods were employed between the process steps to determine the state of the joining zone and the electrical conductivity of the aluminum alloy. The geometries of the co-extruded and then segmented workpieces and the bearing bushings are depicted in Fig. 2.

2.1.1 LACE Process. The LACE tool and the process are described in detail in (Ref 17). For these experiments, the wrought alloy EN AW-6082 was chosen and the reinforcing inner steel tube was made of the ball and roller bearing steel 100Cr6. It had an outer diameter of 44.5 mm and an inner diameter of 32 mm. The extrusion ratio equaled 11:1 in the LACE process.

2.1.2 Die Forging. The die forging tool and the process are described in detail in (Ref 29). For forging, the semi-finished products were extruded using LACE with subsequent machining to the final geometry (∅ 32 inside, ∅ 60.5 mm outside, height 90.9 mm). For preliminary investigations, additional non-extruded, thus unjoined, semi-finished products were also manufactured by machining a steel cylinder (100Cr6, ∅ 32 inside, ∅ 44 mm g6 outside, height 90.9 mm) and an aluminum cylinder (EN AW-6082, ∅ 60.5 mm outside, ∅ 44 mm H7 inside and equal height) with a clearance fit. Before heating, the semi-finished products were coated with a graphite-based lubricant on the aluminum outer sides. Afterward, the bearing bushings were cleaned to ensure no interfering of the graphite with the non-destructive measurements.

2.1.3 Heat Treatment. Due to the multiple heating, forming and cooling operations required for co-extrusion and forging, the aluminum alloy exhibited a non-standard microstructure and heat treatment condition after die forging. Hence, subsequent solution annealing, quenching in water and artificial aging were performed using an electrically heated convection furnace to restore the aluminum alloy to a T6 condition. For solution annealing, the EN AW-6082 alloy has to be heated to temperatures between 500 and 540 °C. These temperatures foster the growth of intermetallic phases in the joining zone. In previous investigations it was found that at a solution annealing temperature of 500 °C, the growth rate of the intermetallic phases was sufficiently reduced compared to a

temperature of 540 °C and, at the same time, it was possible to achieve adequate strength of the aluminum component (Ref 30). To identify suitable heat treatment conditions, four forged bearing bushings were cut into segments using electrical discharge machining, cf. Fig. 2. The microstructural properties of the bearing bushings can differ depending on the position along the axis of the extrusion profile from which these originated (see section. 2.1.1). By dividing the bearing bushings into four segments, an identical heat treatment could be applied to different bearing bushings as well as different heat treatments for the same bearing bushing. For reference, one segment per bushing was not heat treated to characterize the as-fabricated condition after die forging. Four thermocouples were placed near the joining zones of two segments to monitor the temperature on the sample surfaces over the heating time. For temperature measurement, holes were drilled perpendicular to the surface up to the joining zone in the steel and the aluminum sections and the thermocouples were then glued in place with conductive cement. The furnace temperature was set to 500 °C. After 25 min in the furnace, a temperature of 500 °C was reached at all four thermocouple locations. Experiments with different solution annealing times for the T6 heat treatment were carried out on the other segments. Thereby, one segment per bearing bushing, i.e., four pieces per heat treatment, were solution annealed using a solution annealing time of 5 min (heat treatment 1), 15 min (heat treatment 2), 25 min (heat treatment 3) or 35 min (heat treatment 4) were chosen. The segments were quenched in a water bath and then directly artificially aged in second furnace at 150 °C for 24 h.

2.2 Metallographic Examinations

Light-microscope images were taken using a Leica DM4000M microscope (OLYMPUS, Tokyo, Japan) of metallographically ground and polished cross sections. A Scanning Electron Microscope (SEM) Supra 55VP (CARL ZEISS AG, Oberkochen. Germany) was used for higher resolutions images of the ground and polished cross sections and energy dispersive x-ray diffraction (EDX) was employed to map the element distribution.

2.3 Hardness Measurements

Hardness measurements (HV0.5, Force of 4.903 N) were conducted using a hardness tester Q10A + (VERDER SCIENTIFIC GmbH, Haan, Germany) before and after the heat treatment on the segments presented in Fig. 2. A strongly deformed area, position 4 in Fig. 2(b), and a lightly deformed area, position 2 in Fig. 2(b), were investigated at six to ten positions. The specimens were embedded in epoxy resin, ground and then polished to a 3 μm finish. They were then fine-machined with a vibratory polishing machine.

2.4 Shear Tests

The shear tests to characterize the bonding strength were carried out on segments according to the test setup described by (Ref 31). The setup was installed in the universal testing machine Type LFEM 100 from WALTER + BAI AG, (ZWICKROELL GmbH & Co KG, Ulm, Germany. The test speed of the punch was 2 mm/min and the pre-load force was 100 N. The thickness of the specimen was determined using a caliper gauge. The circular arc of the joining zone was previously measured by laser microscope VR-3200 laser microscope (KEYENCE, Osaka, Japan) so that the area of the bonding zone was known and shear stresses could be determined with the values from the installed load cell. The measurement accuracy of the laser microscope for the width measurement was $\pm$ 5 μm.

For the examination, the bearing bushings were first divided into six segments elements of equal size from areas 1 to 5 depicted in Fig. 2(d). The specimens were taken in such a way that the bonding zone in the transition area was as parallel as possible to the force direction of the punch. All specimens were manufactured plane-parallel and the material thickness was 10 mm in each case.

2.5 Non-destructive Testing

Ultrasonic testing and electrical conductivity measurements based on eddy current testing were employed after three process steps, as described in Fig. 1, to characterize the

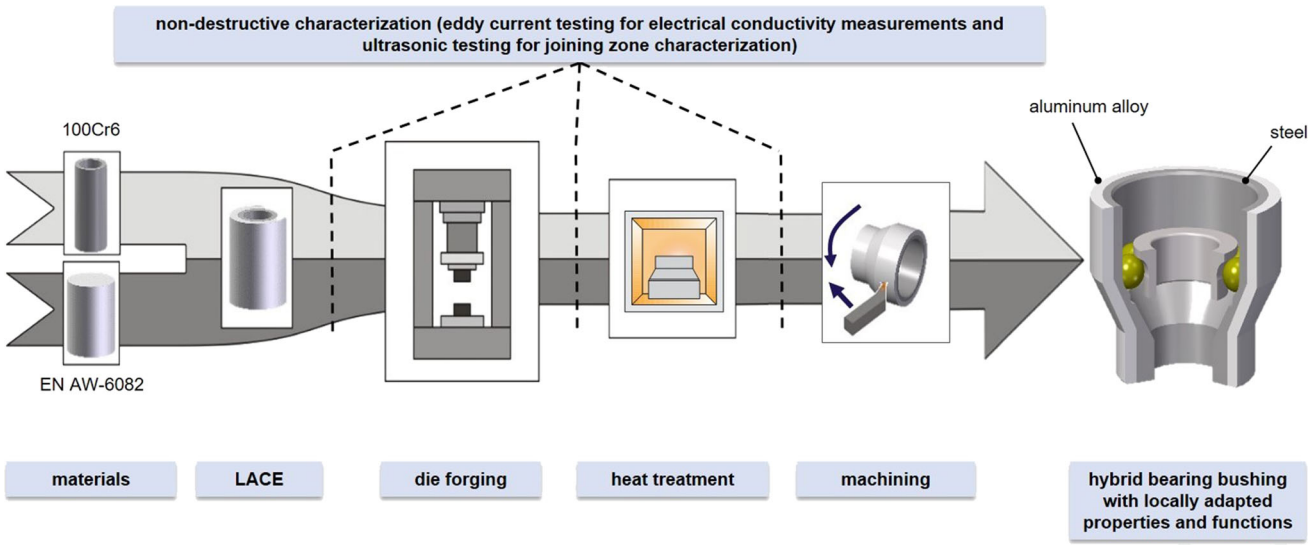


Fig. 1 Process chain to produce a hybrid bearing bushing with locally adapted properties and functions; non-destructive characterization is used between every process step to determine the material and bonding properties

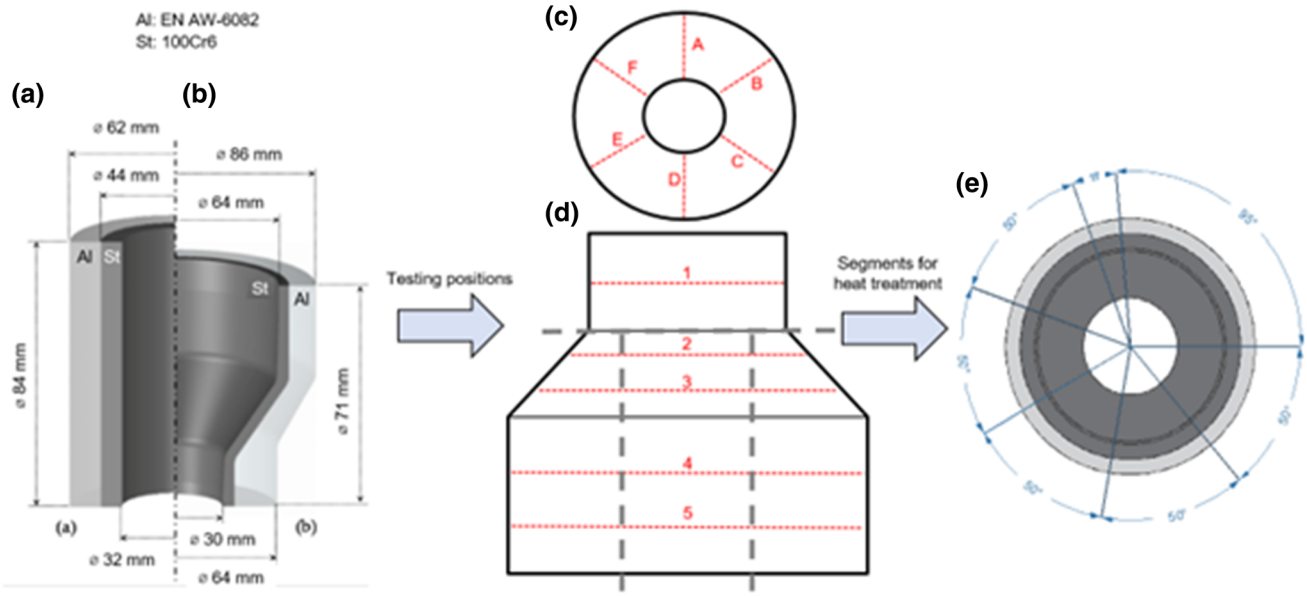


Fig. 2 Geometries of (a) a co-extruded semi-finished hybrid workpiece and (b) a hybrid die-forged bearing bushing consisting of steel (St) and aluminum (Al), measurement positions at the bearing bushing for ultrasonic testing and eddy current testing (c) over the circumference, (d) over the length, gray lines symbolize cuts for segments (e) schematic of the four segments cut from bearing bushings for heat treatment

microstructure and bonding state. Hence, two different part geometries were analyzed, namely the co-extruded semi-finished product and the die-forged bearing bushing, see Fig. 2(a).

In Fig. 2(b), the positions of the measurements for the die-forged samples are depicted. Ultrasonic testing and electrical conductivity measurements were conducted at five positions longitudinally and six positions around the circumference. A similar measuring pattern was applied for the ultrasonic testing of the co-extruded samples. However, the electrical conductivity measurements were conducted at four longitudinal positions on the co-extruded samples as well as 32 positions over the circumference to be able to detect the longitudinal weld seams with high accuracy. For the heat treated samples, only the smaller bearing bushing pieces according to Fig. 2 were tested. That is why only at three positions according to Fig. 2(b) measurement results are displayed.

2.5.1 Ultrasonic Testing. Ultrasonic testing was conducted manually using a USLT 2000 device (Krautkramer, Celle, Germany). An impulse-echo sensor was employed with a diameter of 7.5 mm and was used at a frequency of 15 MHz. Water was used as the coupling agent.

In following, the ultrasonic testing sensor was placed on the aluminum layer. A first echo results from the signal reflected at the backside of the aluminum layer as shown in Fig. 6(a). If there were no bonding at all, only the signal of the aluminum layer would be detected in the ultrasonic impulse-echo measurements. The distance to the first echo equals the thickness of the aluminum component. If the measurement time is long enough, a second echo can be located at four times the thickness of the aluminum. In this case, the signal traveled twice to the backside of the aluminum layer and back to the receiver. The second echo is weaker than the first one due to the damping of the ultrasonic waves inside the material, cf. Fig. 3(a). The red line symbolizes the signal damping. If there is a successfully established joint, the second echo also includes the reflection from the backside of the steel layer. If this is the case, the second echo is higher than the first echo because only a small amount of the ultrasonic wave is reflected on the interface between aluminum and steel and a bigger part is reflected by backside of the steel layer. If the second echo is higher than the first echo, a joining can be assumed, see Fig. 3(b).

2.5.2 Electrical Conductivity Measurements. Electrical conductivity measurements were conducted using a Sigmatest 2.069 device (Foerster, Reutlingen, Germany) with a frequency of 480 kHz and a sensor diameter of 7 mm. Every measurement point was measured probed three times. With the eddy current technology, only the electrical conductivity of non-ferromagnetic materials can be determined. Here, electrical conductivity measurements were used to monitor the microstructural changes in the aluminum alloy. Specifically, precipitations upon artificial aging affect the electrical conductivity, and eddy current technology is a well-known method to monitor the hardening process of aluminum alloys (Ref 25-28). As described by Pankade et al. (Ref 27) the electrical conductivity is the most important parameter associated with hardenable (7xxx) aluminum alloys, and it directly reflects the condition of such alloys. Oliveira et al. (Ref 32) also described that there is a relationship between the electrical conductivity and the heat treatment conditions of 2xxx aluminum alloys. The change in the electrical conductivity is attributed to various precipitation stages resulting from different heat treatment conditions (Ref 27).

3. Results

Figure 4 shows shear strength results after the die forging and prior to the heat treatment, as described in chapter 2.3. The shear strength result are correlated with the ultrasonic testing signals, which were measured before the shear tests. As described in Fig. 3, depending on the height of the second

echo, a good (+) or no bonding (−) was assumed. It can be seen, that the ultrasonic results correlate well with the achieved shear strength.

In Fig. 5, the results of the ultrasonic testing after LACE as well as after the die forging process are presented. Areas where bonding was detected are marked in green, areas with no bonding or insufficient bonding are shown in red. After the LACE process, a homogeneous joint between aluminum and steel is seen. After die forging of the co-extruded sample, local delamination was observed in the highly deformed areas. By contrast, the non-extruded sample, which had the steel tube only placed inside the hollow aluminum cylinder prior to forging, were assumed to have a better bonding in the highly deformed areas. However, in the regions that were not or only slightly deformed by die forging, no bonding was achieved.

The heat treatment did not to have a measureable influence on the boding created by LACE, see Fig. 6. If a debonding was detected, its position was more likely to be in the highly deformed area. In Fig. 7(a) and (c), light-microscopic images of a sample with no joint are displayed. These were taken from the strongly deformed area of the bearing bushing that was previously co-extruded and die-forged. It is evident that a debonding exists between the aluminum alloy and the steel. Figure 8 shows additional EDX measurements and SEM pictures of a debonded area. By contrast, Fig. 7(b) and (d) depicts a bonded structure where an intermetallic phase had formed between the joining partners. These cross sections were taken from a lightly deformed area. In Fig. 8(a), the gray areas between the steel and aluminum are intermetallic phases containing silicon. Figure 8(c) shows the EDX element mapping of an area where no intermetallic phase was formed (e.g., debonded area). Here, oxides get obvious along the steel and aluminum interface.

In addition to ultrasonic testing, the electrical conductivity of the aluminum alloy was monitored at three steps of the process chain to establish a correlation between the processing parameters and the resulting microstructure properties. After the LACE process, see Fig. 9, an elevated electrical conductivity between 29.5 and 31.5 MS/m was detected with a measurement variation of less than 0.25 MS/m for each measurement point taken. As reference, Vetterlein (Ref 33) observed an electrical conductivity for EN AW-6082 of 25-29 MS/m when artificially aged for 0.1-1000 h. However, an elongated region featuring a lower electrical conductivity of about 29.5 MS/m oriented lengthwise can be seen. According to Engelhardt et al. (Ref 28), even small observed variations of the electrical conductivity during tactile eddy current testing can be attributed to locally differing microstructural properties, e.g., in LWS. Hence, it was concluded that the area showing a reduced electrical conductivity is a LWS. This could later on be confirmed in optical micrographs of cross sections etched with hydrofluoric acid.

After die forging, the LWS was no longer detectable. Moreover, the overall electrical conductivity decreased and an inhomogeneous electrical conductivity resulted over the length of the part. The subsequent heat treatment resulted in a further reduced electrical conductivity, see Fig. 9. Here, the electrical conductivities of samples, which were first co-extruded and then die-forged, were measured at the positions 2-4, see Fig. 2(b), before and after the heat treatment. In this case, four different bearing bushings were divided into smaller segments and the four different heat treatments described in chapter 2.1.3 were applied. Positions 1 and 5 have not been analyzed since the samples were cut out of the bearing bushing and shortened for the heat treatment, see Fig. 2. Prior to the heat treatment, elevated electrical conductivities could be determined, see Fig. 10a. After the heat treatment, the electrical conductivity

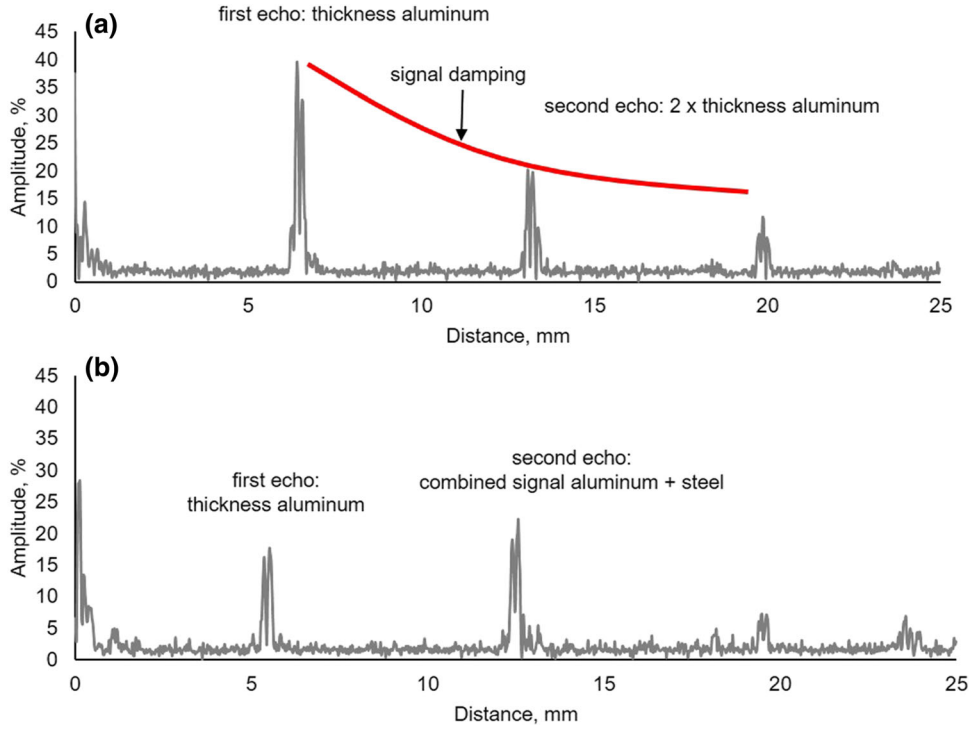


Fig. 3 Exemplary ultrasonic testing signals: (a) when no joining has occurred, (b) when joining between the aluminum and the steel is intense

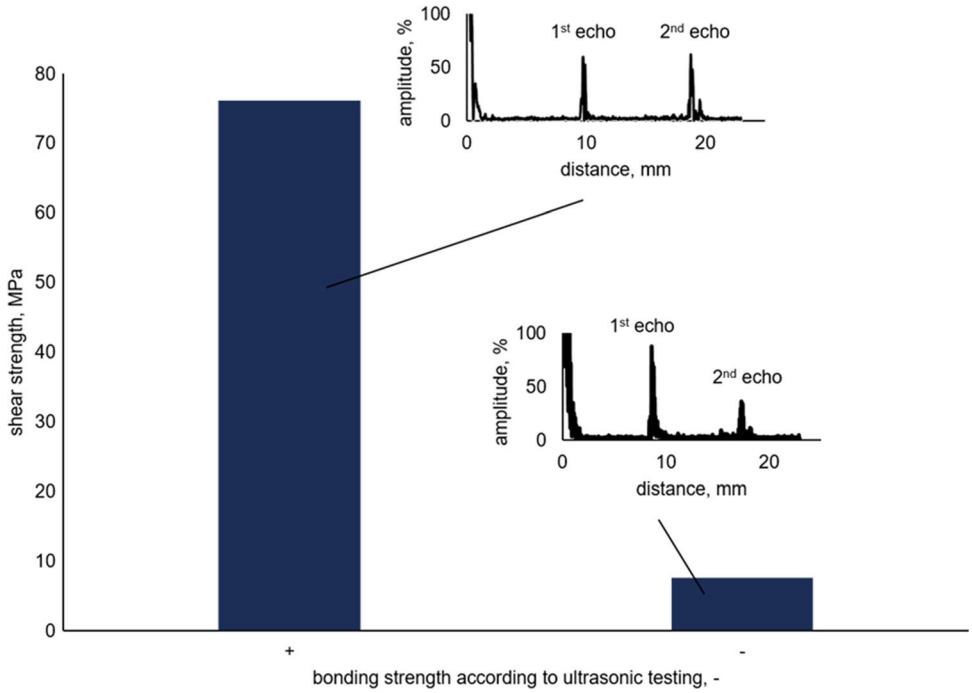


Fig. 4 Correlation between shear strength of pieces of tailored formed bearing bushings and ultrasonic testing signals before the heat treatment

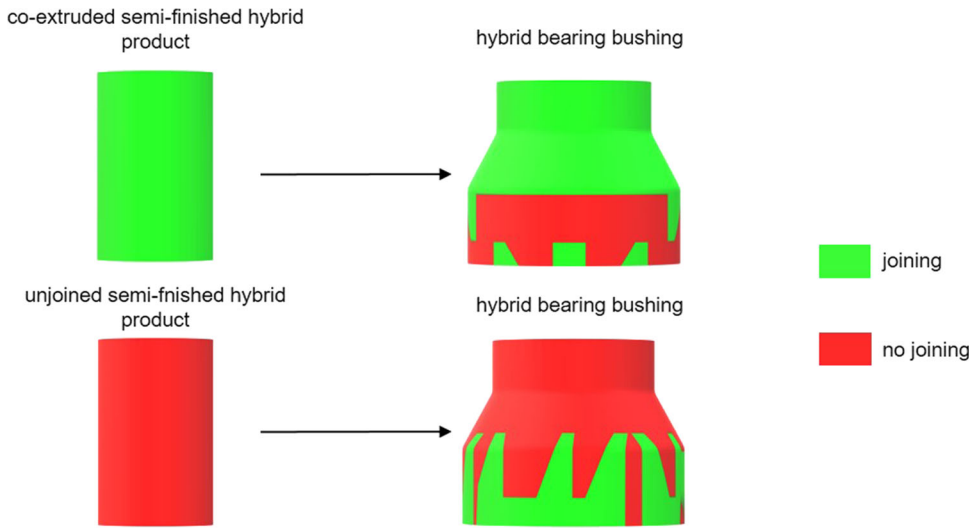


Fig. 5 Ultrasonic testing results for bearing bushings (a) extruded and then die-forged and (b) for unjoined steel and aluminum tubes with subsequent die forging

decreased, cf. Fig. 10(b) and there was no significant difference for the four different heat treatment routes. A similar level of electrical conductivity was observed for all three positions after the heat treatment. Thus, it can be assumed that a homogenous precipitation hardening along the whole sample was achieved.

The electrical conductivity measurements averaged over all three measured positions were supplemented with hardness measurements, see Fig. 11. The heat treatment labeled with zero is the reference condition directly after die forging without any additional heat treatment according to chapter 2.1.3. The hardness increased significantly due to the heat treatments. The hardness measurements reveal that there is only a slight difference between the strongly and lightly deformed areas. This contrasts the electrical conductivity measurements, where a certain difference between the different regions of the bushing is detectable prior to the heat treatment. From the hardness measurements it is clear that even the shortest dwell times (heat treatment 1) during solution annealing were sufficient to establish a T6-condition (Ref 34).

4. Discussion

Ultrasonic testing was applied to analyze the bonding between two metals featuring a similar thickness each as well as similar sound wave speeds. The ultrasonic waves are reflected at boundaries where the material properties of the materials on

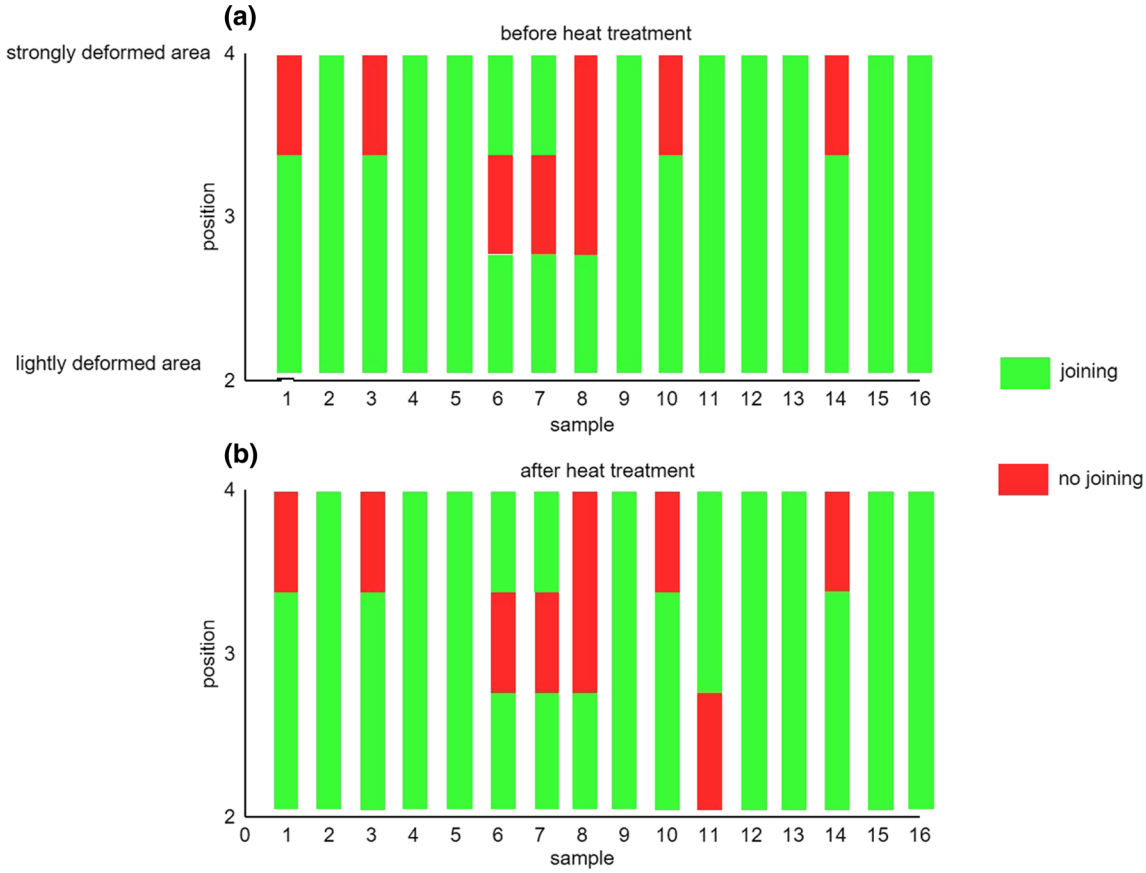


Fig. 6 Ultrasonic testing results for pieces (measurement position 2-4 from Fig. 2(b) of tailored formed bearing bushings (a) before and (b) after the heat treatment

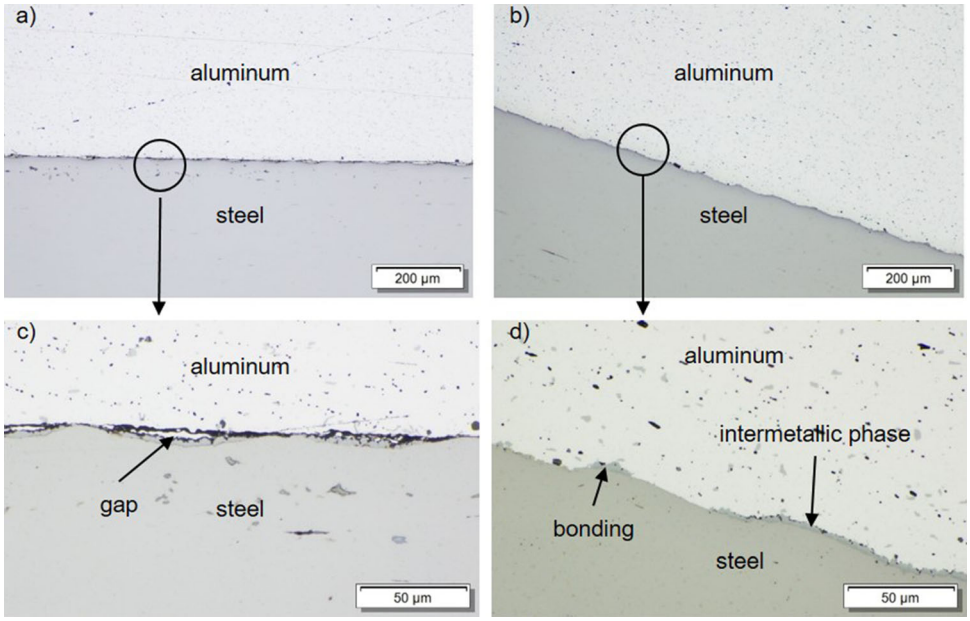


Fig. 7 Metallographic cross sections after heat treatment of highly deformed areas: (a) heat treatment 1, (c) heat treatment 4 and lightly deformed areas, (b) heat treatment 1, (d) heat treatment 4; heat treatments according to chapter 2.1.3

both sides of the interface differ. This difference is often referred to as impedance mismatch. The greater the impedance mismatch, the greater the percentage of energy reflected at the boundary or the boundary between one medium and another medium (Ref 20). This effect can be exploited to correlate the signals with the bonding status of the workpieces. Fortunato

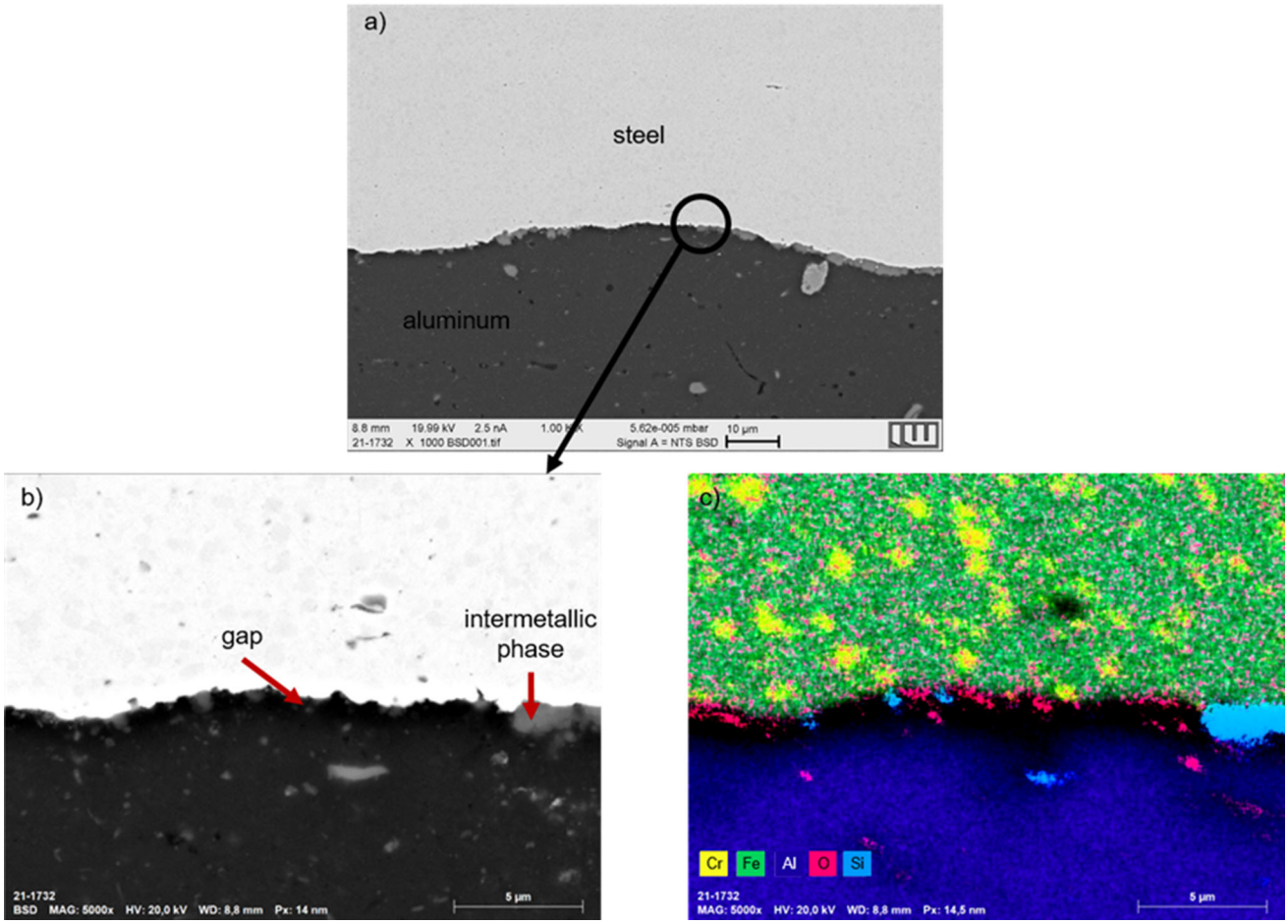


Fig. 8 (a) SEM recordings of Fig. 7(a), (b) selected region for EDX analysis, (c) element mapping of a non-bonded area

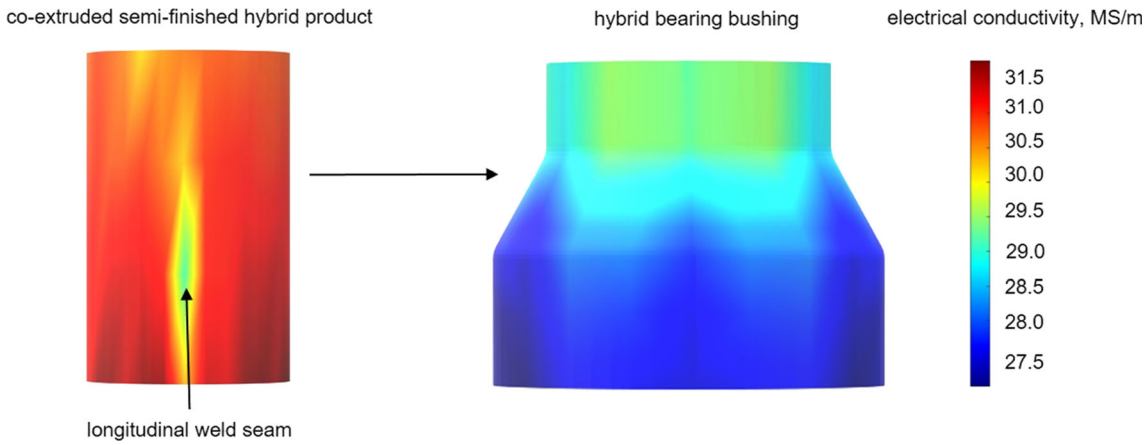


Fig. 9 Electrical conductivity for an extrusion pressed sample and a die-forged bearing bushing

et al. (Ref 22) described that phased array ultrasonic testing is able to detect non-welded specimens but cannot distinguish specimens with major hook defects from specimens correctly weld bonded with small hook defects. Hence, future investigations should focus on the detectable minimum size of possible defects in the bearing bushing production.

The forecast of the bonding quality by ultrasonic testing can be correlated to the shear strength, see Fig. 4. These shows that the analysis of signals presented in Fig. 3 can be used to evaluate the joining zone between aluminum and steel. According to the ultrasonic testing results a homogeneous joining zone was produced after the LACE process (see Fig. 5). Based on previous results, it can be assumed that intermetallic phases like $FeAl_2$, Fe_2Al_5 or $FeAl_3$ have been formed between aluminum and steel (Ref 25, 35, 36). However, no direct correlation of the ultrasonic testing signals to the thickness and type of intermetallic phases was found. Regarding the mechanical properties of the interface, the thickness of the intermetallic

phases is important. Once a certain thickness is exceeded, the mechanical properties decrease significantly (Ref 29). This can result in a failure of the joining zone during the die forging as observed by ultrasonic testing in the strongly deformed sections of the bearing, see Fig. 5. However, when aluminum and steel are forged in the die without an initial connection (see machining condition in Fig. 5), no bond is created if the degree of deformation is insufficient. For such workpieces, bonding only occurs in strongly deformed sections. In some cases, intermetallic phases are formed during die forging due to the elevated forming temperatures (Ref 10, 37). Thus, it can be concluded that stress and heat management in the closed-die forging process can either enhance or prevent a bond between aluminum and steel. For the bearing bushings produced here, this is a major disadvantage, since certain sections of the workpiece show low degrees of deformation, and thus no joint is formed in these areas. Therefore, the use of co-extruded samples is advantageous since a connection already exists prior to the die forging. In this case, however, the process parameters for the highly deformed areas have to be adjusted to prevent deterioration of the bonding. Ultrasonic testing is a useful method to determine the joining status before and after the die forging process. Thus, it can assist to identify suitable die forging parameters to avoid debonding or enhance the joint creation. The information from ultrasonic testing can be used, for example, in numerical simulations (Ref 9) prior to the closed-die forging process, and thus to adapt the process parameters. Here, the inductive heating parameters are of particular importance (Ref 10, 11) since different inductive heating strategies can influence the thickness and nature of the intermetallic phases formed in the bond (Ref 10, 38). Hence, it may be possible to prevent a debonding in the highly deformed regions by adjusting the heating strategy.

Furthermore, it was found that the electrical conductivity of the aluminum alloy was not completely homogeneous along both the sample length and the circumference after the LACE process. This is likely due to local deviations in the microstructure, and thus material properties. For example, it was possible to detect one of the four LWS. Previous investigations showed that typically all weld seams could be localized after the extrusion (Ref 31). After the following die forging process, the LWS was no longer detectable. Hence, it can be concluded that

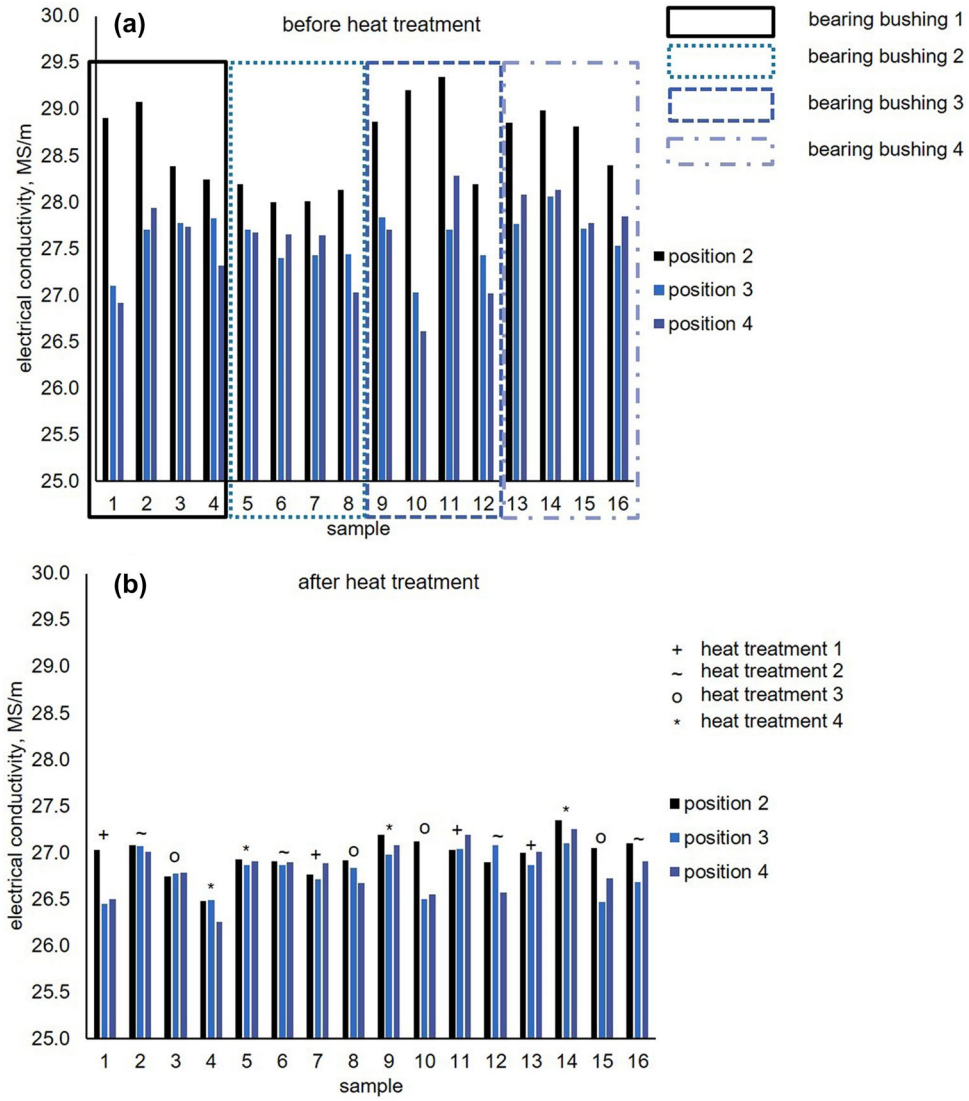


Fig. 10 Electrical conductivity for pieces (measurement position 2-4 from Fig. 2(b)) of tailored formed bearing bushings: (a) before and (b) after the heat treatment, heat treatment according to chapter 2.1.3

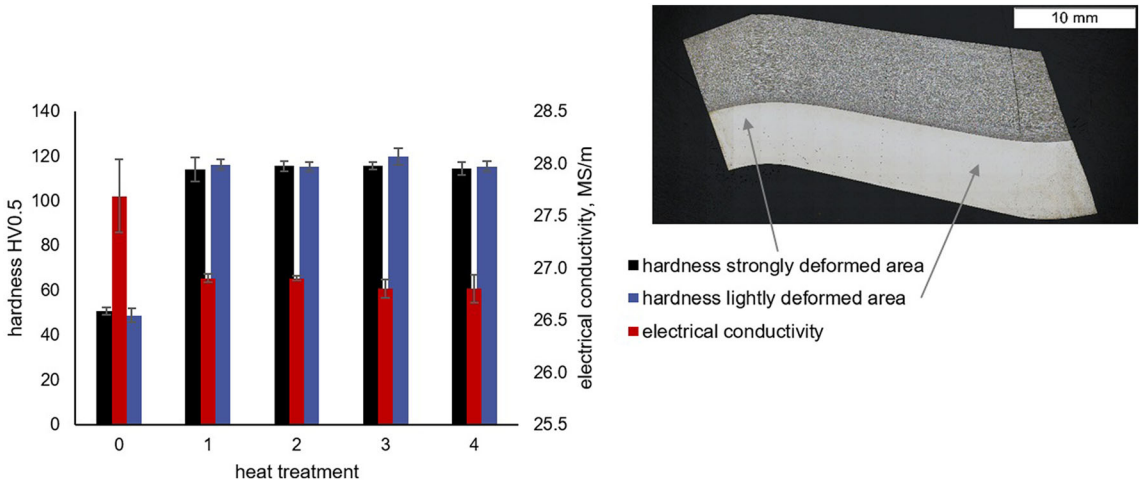


Fig. 11 Hardness measurements before and after the heat treatment (1-4) according to chapter 2.1.3

the heating required for the die forging process results in a certain homogenization of the microstructure in radial direction though the electrical conductivity is decreasing over the bearing bushing length, cf. Fig. 9. Thus, no fully homogeneous microstructure of the aluminum is present. Hence, a heat treatment is required to ensure homogeneous mechanical properties in all aluminum sections of the workpiece.

By the heat treatments conducted, a homogenization of the microstructure was achieved, which could be observed from the measurements of the electric conductivity. However, a longer heating time did not result in a higher electrical conductivity as was described by Uliasz et al. (Ref 26). Hence, the heating times employed here do not seem to influence the aluminum microstructure significantly enough to result in detectable property changes. The hardness of the aluminum alloy increased for all applied heat treatment regimes, which correlates with a reduction in the electrical conductivity and is in accordance with previous observations (Ref 26, 32), cf. Fig. 10 and 11. The correlation between the electrical conductivity and microstructure properties such as grain size, precipitations and especial Guinier-Preston zones, cold hardening effects and solid alloy solutions is very complex (Ref 39) and should be analyzed further. Moreover, it was shown that the subsequent heat treatment has no influence on the joining zone (cf. Fig. 6) to an extent that would be detectable by ultrasonic testing.

Regarding the process chain of Tailored Forming, non-destructive testing is applicable to monitor the evolution of the workpiece status at each individual process steps. By analyzing the joining zone after the LACE process, adaptions of the die forging process to ensure a homogeneous bonding can be facilitated. The subsequent heat treatment is suited to homogenize the aluminum and to reach T6 conditions without a deterioration of the joining zone.

Clearly, non-destructive testing can lay the basis for understanding the influence of different process parameters and enables a step-to-step process control. Further research needs to be performed to find a possibility to characterize the thickness of the intermetallic phases by using non-destructive testing. This in turn would allow improving the bonding and material properties further.

5. Conclusions

Non-destructive testing was employed between three production steps of a process chain used to produce hybrid bearing bushings by Tailored Forming. Using both ultrasonic testing as well as eddy current measurements, changes of the joining zone conditions between the joining partners and the microstructure of the aluminum alloy were monitored. It was found that:

- These non-destructive methods can be used to monitor the component properties after each production step.
- Bonding and aluminum microstructure are dependent on the deformation rate and the time-temperature profile and can be modified by adapting the parameters on basis of the non-destructive testing.
- Pre-joined semi-finished products lead to a detectable bonding in areas at low deformation ratio unlike unjoined semi-finished products.
- Although the heat treatment reproduced the T6 status of the aluminum alloy, no difference in the quality of the bonding in the joining zone was detected by ultrasonic testing.
- Eddy current testing could be used to minimize the heat treatment time by monitoring the microstructure within the heat treatment.
- The heat treatment is homogenizing the microstructure so that no microstructure differences in LWS can be detected with simultaneous not influencing the bonding.

Funding

Open Access funding enabled and organized by Projekt DEAL. This study was funded by the Deutsche Forschungsgemeinschaft (DFG, German Research Foundation)—CRC 1153—252662854, sub-projects A1, A2 and B2. The authors thank the DFG for financial support.

Conflict of interest

The authors declare no conflict of interest.

Open Access

This article is licensed under a Creative Commons Attribution 4.0 International License, which permits use, sharing, adaptation, distribution and reproduction in any medium or format, as long as you give appropriate credit to the original author(s) and the source, provide a link to the Creative Commons licence, and indicate if changes were made. The images or other third party material in this article are included in the article's Creative Commons licence, unless indicated otherwise in a credit line to the material. If material is not included in the article's Creative Commons licence and your intended use is not permitted by statutory regulation or exceeds the permitted use, you will need to obtain permission directly from the copyright holder. To view a copy of this licence, visit http://creativecommons.org/licenses/by/4.0/.

References

1. A. Jamwal, R. Agrawal, M. Sharma, and A. Giallanza, Industry 4.0 Technologies for Manufacturing Sustainability: A Systematic Review and Future Research Directions, *Appl. Sci.*, 2021, **11**, p 5725. https://doi.org/10.3390/app11125725
2. M. Merklein, M. Johannes, M. Lechner, and A. Kuppert, A Review on Tailored Blanks: Production, Applications and Evaluation, *J. Mater. Process. Technol.*, 2014, **214**, p 151–164. https://doi.org/10.1016/j.jmatprotec.2013.08.015
3. L. Agudo, N. Jank, J. Wagner, S. Weber, C. Schmaranzer, E. Arenholz, J. Bruckner, H. Hackl, and A. Pyzalla, Investigation of Microstructure and Mechanical Properties of Steel-Aluminium Joints Produced by Metal Arc Joining, *Steel Res. Int.*, 2008, **79**, p 530–535. https://doi.org/10.1002/srin.200806162
4. S. Mukae, K. Nishio, M. Kato, T. Inoue, and K. Sumitomo, Effect of Heat Treatment on Bond Characteristics of Aluminium Clad Steel: Production and Characteristics Of Vacuum Roll Bonded Clad Materials (2nd Report), *Weld. Int.*, 1995, **9**, p 384–389. https://doi.org/10.1080/09507119509548817
5. G. Sierra, P. Peyre, F. Deschaux-Beaume, D. Stuart, and G. Fras, Steel to aluminium Key-Hole Laser Welding, *Mater. Sci. Eng. A*, 2007, **447**, p 197–208. https://doi.org/10.1016/j.msea.2006.10.106
6. M. Ashfaq, N. Sajja, H. Khalid Rafi, and R.K. Prasad, Improving Strength of Stainless Steel/Aluminum Alloy Friction Welds by Modifying Faying Surface Design, *J. Mater. Eng. Perform.*, 2013, **22**, p 376–383. https://doi.org/10.1007/s11665-012-0278-0
7. K. Kimapong, and T. Watanabe, Lap Joint of A5083 Aluminum Alloy and SS400 Steel by Friction Stir Welding, *Mater. Trans.*, 2005, **46**, p 835–841. https://doi.org/10.2320/matertrans.46.835
8. T. Watanabe, H. Takayama, and A. Yanagisawa, Joining of Aluminum Alloy to Steel by Friction Stir Welding, *J. Mater. Process. Technol.*, 2006, **178**, p 342–349. https://doi.org/10.1016/j.jmatprotec.2006.04.117
9. B.-A. Behrens, H.J. Maier, G. Poll, P. Wriggers, F. Aldakheel, C. Klose, F. Nürnberger, F. Pape, C. Böhm, A. Chugreeva, T. Coors, D. Duran, S. Thürer, S. Herbst, J.-I. Hwang, T. Matthias, N. Heimes, and J. Uhe, Numerical Investigations Regarding a Novel Process Chain for the Production of a Hybrid Bearing Bushing, *Prod. Eng. Res. Devel.*, 2020, **14**, p 569–581. https://doi.org/10.1007/s11740-020-00992-7
10. B.A. Behrens, J. Uhe, T. Petersen, C. Klose, S. Thürer, J. Diefenbach, and A. Chugreeva, Challenges in the Forging of Steel-Aluminum Bearing Bushings, *Materials*, 2021, **14**, p 803. https://doi.org/10.3390/ma14040803
11. Q.Y. Lu, and C.H. Wong, Additive Manufacturing Process Monitoring and Control by Non-destructive Testing Techniques: Challenges and In-process Monitoring, *Virtual Phys. Prototyping*, 2018, **13**(2), p 39–48. https://doi.org/10.1080/17452759.2017.1351201
12. B.-A. Behrens, A. Chugreeva, J. Diefenbach, C. Kahra, S. Herbst, F. Nürnberger, and H.J. Maier, Microstructural Evolution and Mechanical Properties of Hybrid Bevel Gears Manufactured by Tailored Forming, *Metals*, 2020, **10**, p 1365. https://doi.org/10.3390/met10101365
13. M. Bernard, Ch. Scheer, V. Böhm, W. Reimche, and F.-W. Bach, New Developments in Non-destructive Testing for Quality Assurance in Component Manufacturing, *Steel Res. Int.*, 2009, **80**(12), p 916–924. https://doi.org/10.2374/SRI09SP144
14. J. Hefele, and R.D. Bolton, Non-destructive Tracing of a Product Life Cycle Through Geometry Extraction from Radiographs, *Global Engineering, Manufacturing and Enterprise Networks*. J.P.T. Mo, L. Nemes Ed., Springer, Boston, 2001, p 291–297
15. N. Melchert, M.K.-B. Weiss, T. Betker, W. Frackowiak, R. Gansel, L. Keunecke, E. Reithmeier, H.J. Maier, M. Kästner, and D. Zaremba, Combination of Optical Metrology and Non-destructive Testing Technology for the Regeneration of Aero Engine Components, *tm Technisches Messen*, 2021, **88**, p 237–250. https://doi.org/10.1515/teme-2020-0093
16. B. Wolter, G. Dobmann, and C. Boller, NDT Based Process Monitoring and Control, *SV-JME*, 2011, **2011**, p 218–226. https://doi.org/10.5545/sv-jme.2010.172
17. S.E. Thürer, A. Chugreeva, N. Heimes, J. Uhe, B.-a Behrens, H.J. Maier, and C. Klose, Process Chain for the Manufacture of Hybrid Bearing Bushings, *Prod. Eng. Res. Devel.*, 2021, **15**, p 137–150. https://doi.org/10.1007/s11740-021-01028-4
18. H. Valberg, Extrusion Welding in Aluminium Extrusion, *Int. J. Mater. Prod. Technol.*, 2002, **17**, p 497–556. https://doi.org/10.1504/IJMPT.2002.001317
19. G. Rosa, P. Psyllaki, R. Oltra, T. Montesin, C. Coddet, and S. Costil, Laser Ultrasonic Testing for Estimation of Adhesion of Al_2O_3 Plasma Sprayed Coatings, *Surf. Eng.*, 2001, **17**, p 332–338. https://doi.org/10.1179/026708401101517881
20. J. Zhang, Y. Cho, J. Kim, A.K. Malikov, Y.H. Kim, J.-H. Yi, and W. Li, Non-Destructive Evaluation of Coating Thickness Using Water Immersion Ultrasonic Testing, *Coatings*, 2021, **11**, p 1421. https://doi.org/10.3390/coatings11111421
21. F. Bastianini, A. Di Tommaso, and G. Pascale, Ultrasonic Non-destructive Assessment of Bonding Defects in Composite Structural Strengthenings, *Compos. Struct.*, 2001, **53**, p 463–467. https://doi.org/10.1016/S0263-8223(01)00058-7
22. J. Fortunato, C. Anand, D.F.O. Braga, R.M. Groves, P.M.G.P. Moreira, and V. Infante, Friction Stir Weld-Bonding Defect Inspection using Phased Array Ultrasonic Testing, *Int. J. Adv. Manuf. Technol.*, 2017, **93**, p 3125–3134. https://doi.org/10.1007/s00170-017-0770-7
23. Y. Bar-cohen, A.K. Mal, and C.C. Yin, Ultrasonic Evaluation of Adhesive Bonding, *J. Adhes.*, 1989, **29**, p 257–274. https://doi.org/10.1080/00218468908026491
24. B. Yılmaz, and E. Jasiūnienė, Advanced Ultrasonic NDT for Weak Bond Detection in Composite-Adhesive Bonded Structures, *Int. J. Adhes. Adhes.*, 2020, **102**, p 102675. https://doi.org/10.1016/j.ijadhadh.2020.102675
25. M. Yılmaz, M. Çöl, and M. Acet, Interface Properties of Aluminum/Steel Friction-Welded Components, *Mater. Charact.*, 2002, **49**, p 421–429. https://doi.org/10.1016/S1044-5803(03)00051-2
26. P. Uliasz, T. Knych, M. Piwowarska, and J. Wiechec, The Influence of Heat Treatment Parameters on the Electrical Conductivity of AlSi7Mg and AlSi10Mg Aluminum Cast Alloys, *ICAA13 Pittsburgh*. H. Weiland, A.D. Rollett, W.A. Cassada Ed., Springer, Cham, 2016, p 129–135
27. S.B. Pankade, D.S. Khedekar, and C.L. Gogte, The Influence of Heat Treatments on Electrical Conductivity and Corrosion Performance of AA 7075-T6 Aluminium Alloy, *Proc. Manuf.*, 2018, **20**, p 53–58. https://doi.org/10.1016/j.promfg.2018.02.007
28. M. Engelhardt, N. Grittner, W. Reimche, and F.W. Bach, Non-Destructive Detection of Weld Seams in Extruded Aluminum Profiles, *KEM*, 2013, **585**, p 103–110. https://doi.org/10.4028/www.scientific.net/KEM.585.103
29. B.-A. Behrens, V. Sokolinskaja, A. Chugreeva, J. Diefenbach, S. Thürer, and D. Bohr, Investigation into the Bond Strength of the Joining Zone of Compound Forged Hybrid Aluminium-Steel Bearing Bushing, *AIP Conf. Proc.*, 2019, **2113**, p 40028. https://doi.org/10.1063/1.5112562
30. S. Herbst, H. Aengeneyndt, H.J. Maier, and F. Nürnberger, Microstructure and Mechanical Properties of Friction Welded Steel-Aluminum Hybrid Components after T6 Heat Treatment, *Mater. Sci. Eng. A*, 2017, **696**, p 33–41. https://doi.org/10.1016/j.msea.2017.04.052
31. S.E. Thürer, J. Peddinghaus, N. Heimes, F.C. Bayram, B. Bal, J. Uhe, B.-A. Behrens, H.J. Maier, and C. Klose, Lateral Angular Co-Extrusion: Geometrical and Mechanical Properties of Compound

Profiles, *Metals*, 2020, **10**, p 1162. https://doi.org/10.3390/met10091162

32. P.J. Oliveira, M.L.N. Melo, R.S.M. Silva, and D.O. Caixeta, Relationship between Electrical Conductivity and the Stage of the Heat Treatments of Aging and Overaging of the Aluminum Alloy AA2024, *MSF*, 2018, **930**, p 400–404. https://doi.org/10.4028/www.scientific.net/MSF.930.400
33. J. Vetterlein, Charakterisierung von Wärmebehandlungszuständen in Aluminiumlegierungen durch In-situ-Wirbelstrommessung. PhD Thesis, 2008
34. DIN EN 755-2:2016 Aluminium und Aluminiumlegierungen: Stranggepresste Stangen, Rohre und Profile - Teil 2: Mechanische Eigenschaften (755-2:2016)
35. B.-A. Behrens, H.J. Maier, C. Klose, H. Wester, S.E. Thürer, N. Heimes, and J. Uhe, Characterization and Modeling of Intermetallic Phase Formation during the Joining of Aluminum and Steel in Analogy to Co-Extrusion, *Metals*, 2020, **10**, p 1582. https://doi.org/10.3390/met10121582
36. B. Sundman, I. Ohnuma, N. Dupin, U.R. Kattner, and S.G. Fries, An Assessment of the Entire Al-Fe System Including D03 Ordering, *Acta Mater.*, 2009, **57**, p 2896–2908. https://doi.org/10.1016/j.actamat.2009.02.046
37. B.-A. Behrens and K.-G. Kosch, Influence of Different Alloying Elements on the Intermetallic Phase Seam Thickness of Compound Forged Steel-Aluminum Parts, *Prod. Eng. Res. Devel.*, 2011, **5**, p 517–522. https://doi.org/10.1007/s11740-011-0327-9
38. S. Wohletz and P. Groche, Temperature Influence on Bond Formation in Multi-material Joining by Forging, *Proc. Eng.*, 2014, **81**, p 2000–2005. https://doi.org/10.1016/j.proeng.2014.10.271
39. W. Hufnagel, *Aluminium-Taschenbuch*, 14th ed. Aluminium-Verlag GmbH, Düsseldorf, 1988

Publisher's Note Springer Nature remains neutral with regard to jurisdictional claims in published maps and institutional affiliations.